

Absence of Fermi surface reconstruction in pressure-driven overdoped YBCO

Stanley W. Tozer,^{1,*} William A. Coniglio,¹ Tobias Förster,² Doug A. Bonn,³ Walter N. Hardy,³ Ruixing Liang,³ Erik Kampert,^{2,4} and Audrey D. Grockowiak^{1,5,6}

¹*National High Magnetic Field Laboratory (NHMFL), Florida State University, Tallahassee, Florida*

²*Hochfeld-Magnetlabor Dresden (HLD-EMFL), Helmholtz-Zentrum Dresden-Rossendorf, 01328, Dresden, Germany*

³*Department of Physics and Astronomy, University of British Columbia, Vancouver, British Columbia V6T 1Z4, Canada*

⁴*Institute of Fundamentals of Electrical Engineering,*

Helmut Schmidt University, 22043 Hamburg, Germany

⁵*Brazilian Synchrotron Light Laboratory (LNLS/Sirius),*

Brazilian Center for Research in Energy and Materials (CNPEM), Campinas, Brazil

⁶*Leibniz-Institut für Festkörper- und Werkstofforschung Dresden, 01069 Dresden, Germany*[†]

(Dated: December 5, 2023)

The evolution of the critical superconducting temperature and field, quantum oscillation frequencies and effective mass m^* in underdoped $\text{YBa}_2\text{Cu}_3\text{O}_{7-\delta}$ (YBCO) crystals ($p = 0.11$, with p the hole concentration per Cu atom) points to a partial suppression of the charge orders with increasing pressure up to 7 GPa, mimicking doping. Application of pressures up to 25 GPa pushes the sample to the overdoped side of the superconducting dome. Contrary to other cuprates, or to doping studies on YBCO, the frequency of the quantum oscillations measured in that pressure range do not support the picture of a Fermi-surface reconstruction in the overdoped regime, but possibly point to the existence of a new charge order.

INTRODUCTION

The pnictides, cuprates, and molecular conductors exhibit similar features, leading to the possibility of a common mechanism anchored in a universal phase diagram. Typical ingredients for such phase diagrams include an antiferromagnetic phase, one or more superconducting domes, and possibly one, or several quantum critical points (QCP). Chemical doping is a traditional means to look at such phenomena.

The temperature-oxygen doping phase diagram of $\text{YBa}_2\text{Cu}_3\text{O}_{7-\delta}$ (YBCO) is extremely rich and exhibits a narrow antiferromagnetic region at the lowest doping. At higher doping, a superconducting dome develops [1] with a hole doping of $p = 0.05$ at the onset. The dome extends up to $p = 0.17$, which corresponds to optimal doping, past which no samples are available. A shoulder at $p = 0.08$ is associated with a Fermi surface reconstruction (FSR) [2] as indicated by a change in sign of the Hall [3],[4] and Seebeck coefficients [5] from positive to negative at low temperatures, as well as at high magnetic fields. This change in sign has been attributed, by utilizing nuclear magnetic resonance (NMR) [6] and x-ray diffraction (XRD) [7], to the presence of a two-dimensional charge order with a maximum around $p = 0.12$. Subsequently, a field induced three-dimensional charge order (CO) was revealed by XRD [8], ultrasound [9], and NMR measurements [10] in the same doping range. This has been recreated in zero field by the application of uniaxial strain along the a -axis of its orthorhombic structure [11].

It is widely accepted that the Fermi surface (FS) undergoes a second reconstruction with oxygen doping, small electron and hole pockets evolving to arcs [12] and

finally to a large pocket on the overdoped side [13],[14]. This picture is drawn from looking at the charge-carrier concentration in the copper-oxygen planes, and by comparing various cuprates at different doping levels with $\text{Tl}_2\text{Ba}_2\text{CuO}_{6+\delta}$, the overdoped analogue to YBCO [15]. This is further supported by angle-resolved photoemission spectroscopy (ARPES) measurements of underdoped $\text{YBa}_2\text{Cu}_3\text{O}_{6.5}$ (YBCO6.5) crystals. These studies [16] have shown that the surface is naturally overdoped and different from the bulk, having found large Fermi arcs instead of the pockets measured via Shubnikov-de Haas (SdH) [12]. By depositing K^+ ions on the surface, the authors reduced the charge-carrier doping at the surface and recovered the small Fermi-surface pockets [16]. The only study showing a Fermi surface reconstruction (FSR), from underdoped to overdoped within one material, was carried out on the electron-doped $\text{Nd}_{2-x}\text{Ce}_x\text{CuO}_4$ compound via SdH measurements [17].

Additionally, fermiology studies of various oxygen dopings in YBCO have revealed a divergence of the effective mass of the charge carriers close to optimal doping, hinting at the existence of a quantum critical point (QCP) under the superconducting dome [18]. The relationship between this putative QCP and the FSR is not completely established.

Both the QCP and the FSR are crucial to our understanding of the cuprates as well as the universal phase diagram. A study of the Fermi surface via quantum oscillations (QO), with the aim of observing a reconstruction, requires suppressing the superconducting phase to look at the normal state of the material

close to optimal doping, and beyond. Ideally, high magnetic fields are used to suppress superconductivity allowing for the observation of QO in the vicinity of the QCP; however, due to the high superconducting critical transition temperature (T_c) and concomitant superconducting critical field (H_{c2}), this would require fields in excess of 100 T [19], beyond that currently available in non-destructive magnets. Instead, doping with Zn up to $p=0.22$ has been used to suppress the superconducting dome to a maximum T_c of about 30 K [20], but doping to these levels introduces impurities and thus scattering which precludes the observation of QO.

To date, high pressure studies look mostly at the evolution of T_c with pressure [21], [22], [23], [24]. Here, we have used quasi-hydrostatic pressure to tune the FS of YBCO6.5 starting from the underdoped region, $p=0.11$, and progressing through the superconducting dome. Measuring the evolution of QO with pressure and temperature provided direct access to the FSs and the effective masses of the charge carriers, which showed a lack of Fermi surface reconstruction, and possibly points instead to the existence of a charge order similar to the that found on the underdoped side.

EXPERIMENTAL METHODS

We have used high purity twinned single crystals of YBCO6.5 ($p=0.11$) to perform high magnetic field Shubnikov-de Haas measurements under high pressure. Our experiments were carried out between 350 mK and 10 K in DC fields up to 45 T and pressures up to 25 GPa at the NHMFL using metallic diamond anvil cells (DACs), and in pulsed fields up to 80 T and 7 GPa at HDL-EMFL using plastic DACs [25], rotators, and cryogenic tails. The sample is coupled to a resonant LC tank circuit driven by a tunnel diode oscillator (TDO). The small coil that makes up the inductor of this LC circuit resides in the high pressure volume of the DAC and senses changes in sample resistivity due to variations in temperature, pressure, or magnetic field (see supplementary information). This allowed us to develop a field-pressure-temperature phase diagram. All data is taken with the c -axis of the crystal oriented parallel to the magnetic field.

RESULTS

Pressure effect on T_c in zero field

In our study, the pressure was changed at room temperature, and was only increased during the course of this work, i.e. no measurements upon decompression were performed. The large vertical thermal gradient ex-

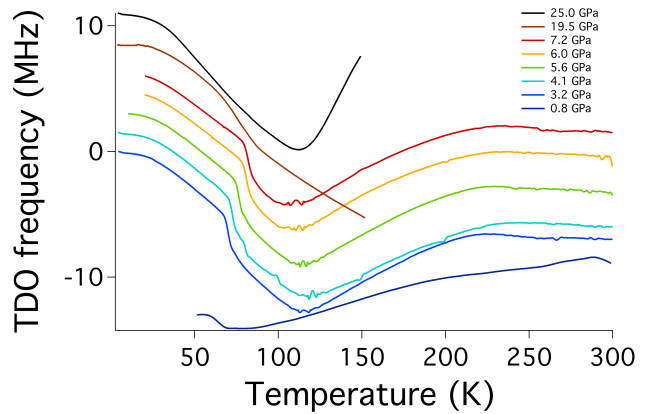


Figure 1: Evolution of the TDO frequency as a function of temperature for several pressures at 0 T. The kink around 80 K is interpreted as the superconducting transition, and T_c is taken as the minimum in the derivative of the signal in that temperature range as shown in Sup. Fig. 2. The observed kinks in those curves cannot be interpreted as T_c as they are not suppressed with field as shown in Sup. Fig. 7). No clear transition appears at 25 GPa. The minima observed in the signals at 115 K is an experimental artifact due to cross-over of frequency mixing.

isting in cryostats upon loading a probe in DC fields or pulsed magnets makes any accurate determination of T_c difficult and time constrains did not allow for controlled warming of the sample during high field time. Careful T_c measurements were performed in a ^4He , 16 T Quantum Design PPMS, with the pressure being measured at the transition temperature. Figure 1 shows the evolution of the TDO frequency with temperature for various pressures. We define T_c as the minimum of the derivative of the signal around 80 K for the pressures up to 7.2 GPa, over which range T_c smoothly increases up 81.2K. At 19.5 GPa, T_c decreases to 75 K, pointing to the sample having been driven to the overdoped side of the superconducting dome. At 25 GPa, we do not observe a similar kink down to 2 K in the PPMS. The minimum around 100 K in the 25 GPa cell in Fig. 1 cannot be interpreted as a T_c , as applied fields of 16 T did not shift it to lower temperatures (Sup. Fig. 5). Rather a combination of non-hydrostaticity, and pressure variation upon cooling can explain the lack of T_c at that pressure., both of which tend to broaden transitions which make T_c more difficult to measure. The cells used at higher pressure also have a larger variation in pressure with temperature: we measured an increase in pressure of roughly 20% between room temperature and ^4He temperatures.

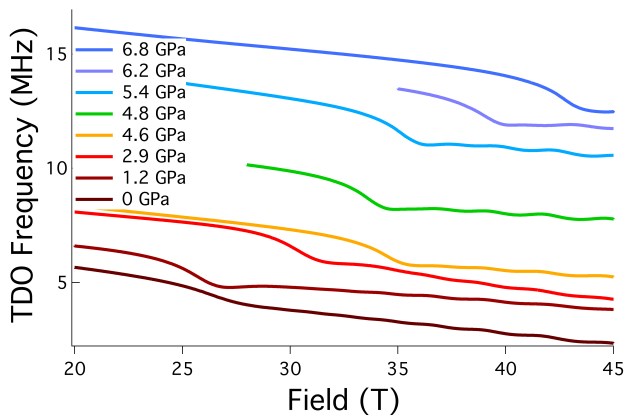


Figure 2: TDO frequencies as a function of magnetic field for several pressures at 400 mK. The TDO frequencies are vertically shifted for clarity. QOs are clearly visible above the critical field.

Pressure effect on the critical field

Pressures lower than 10 GPa

The TDO frequencies as a function of the magnetic field measured in the 45 T hybrid magnet are plotted in Fig. 2 for various pressures at approximately 400 mK. A clear trend in H_{c2} appears, dramatically increasing in a non-monotonic fashion up to 6.8 GPa, where H_{c2} is about 44 T. The 45 T hybrid magnet limits our QO study to about 6 GPa for the underdoped side of the superconducting dome of YBCO. Pulsed magnetic fields are required to measure the evolution of H_{c2} and the QO frequencies for the higher pressure range.

Figure 3 shows an example of data obtained in a 70 T magnet at 500 mK during a 150 ms pulse for a YBCO_{6.5} sample at 0.8 GPa. The main panel shows the as-measured TDO frequency, where the transition at about 25 T is identified as the superconducting critical field H_{c2} in agreement with other resistivity data in the literature [19]. Above this transition, clear QOs are observed in the data, and thus we will use this as the marker for H_{c2} throughout this work. The two traces correspond to the data taken during the up and down sweep in magnetic field, with overlapping traces indicating that there is no heating of the sample during the pulse. The background-subtracted data above H_{c2} is shown in the top right-hand corner panel, with one frequency clearly observed, confirmed by the FFT (bottom left). Similar data were obtained up to 7 GPa in a 85 T magnet, shown in Sup. Fig. 3.

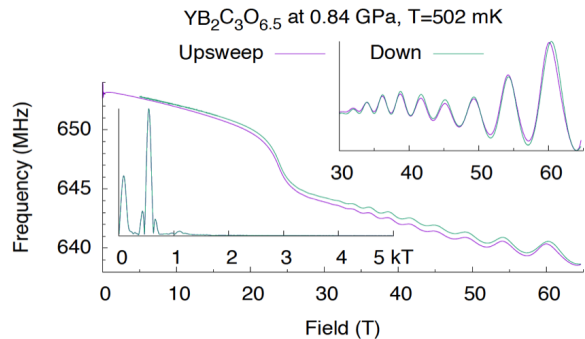


Figure 3: Main panel: TDO frequency as a function of magnetic field for a sample at 502 mK and 0.84 GPa. Top right panel: oscillatory-part background-subtracted data above H_{c2} . Bottom left panel: FFT of the background subtracted data. The lower frequency peak is a data analysis artifact coming from the polynomial background subtraction.

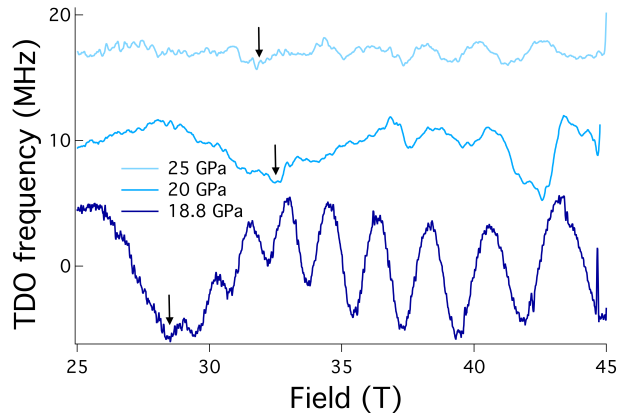


Figure 4: Base ³He temperature, background-subtracted TDO frequency as a function of field for three pressures. The sample in the 20 GPa cell was bridged, leading to poorer quality data. H_{c2} is indicated with arrows and determined by the onset field at which QOs appear. The traces are vertically shifted for clarity.

Pressures greater than 18 GPa

The estimated values of H_{c2} as one approaches optimal doping are greater than the magnetic fields available in non-destructive pulsed magnets, therefore higher pressures were used to drive the sample to the overdoped side. For this purpose, three different pressure cells loaded with a 4:1::methanol:ethanol mixture were taken to higher pressures (18.8, 20.0 and 25 GPa) at low temperatures. In a related study, Alireza *et al.* [21] used a similar approach and reconstructed the overdoped side of the superconducting dome by applying pressures of

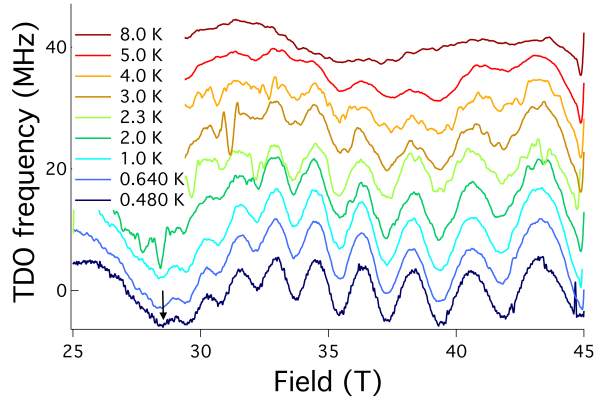
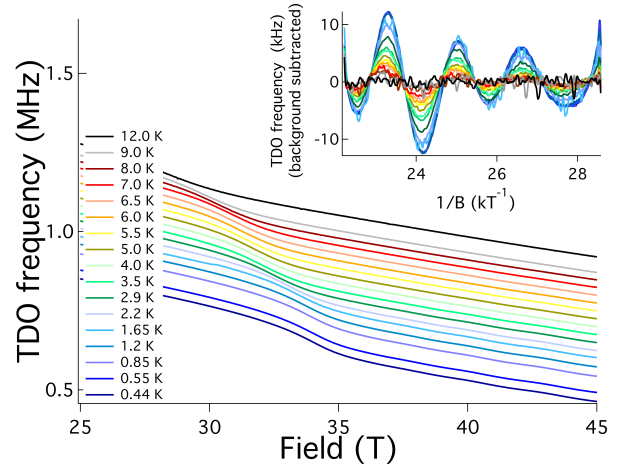


Figure 5: Evolution of the background-subtracted TDO frequency as a function of field for various temperatures at 18.8 GPa at low temperature. We assign the minimum in the signal before the onset of the QOs to H_{c2} , indicated by an arrow. The various traces are vertically shifted for clarity.

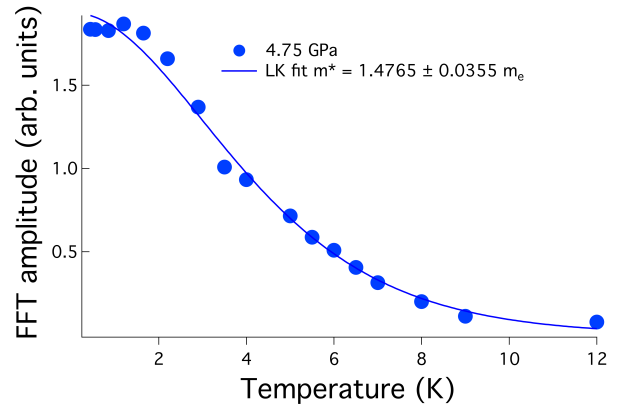
about 25 GPa to an optimally doped sample $p = 0.17$. Figure 4 shows the background-subtracted TDO-frequency field dependence of our sample at base ^3He temperatures. The 18.8 GPa cell shows a clear minimum in the signal at 28.4 T (indicated by an arrow) followed by the onset of QO. Again, we identify this minimum as the critical field. This feature is not as pronounced for higher pressures, but QO are still observable. Figure 5 shows the evolution of the background-subtracted TDO frequency as a function of field for various temperatures for YBCO6.5 at 18.8 GPa. The critical field is clearly suppressed with increasing temperature. We plot H_{c2} vs temperature for various pressures in Sup. Fig. 7, and show that the temperature dependence of the transition at 18.8 GPa follows the same trend.

High pressure fermiology

For each pressure, field sweeps were performed at various temperatures to study the temperature dependence of the QO amplitude, as shown in Fig. 6(a) for 4.8 GPa and in Sup. Fig. 8 for 25 GPa. The oscillatory part is plotted as a function of $1/B$, interpolated and smoothed with a Savitzky-Golay filter [26]. A smooth background is subtracted, and the FFT of the result is taken using a Hamming window. The amplitude $A(T)$ of each Fourier transform peak is then plotted versus temperature as shown in Fig. 6(b), and fitted using the Lifshitz-Kosevitch (LK) theory (1) for the temperature damping



(a)



(b)

Figure 6: (a) TDO frequency at 4.8 GPa as a function of field for various temperatures, vertically shifted for clarity. These traces are background-subtracted in the oscillatory region and plotted as a function of the inverse field in the insert. The amplitude of the peak of the Fourier transform of these background-subtracted traces is fitted with a Lifshitz-Kosevitch equation in (b), yielding the effective mass of the carriers. The deviation to the LK observed at temperatures below 1.4 K can be ascribed to heating due to the TDO.

factor [27]:

$$A(T) = A_0 \frac{\alpha m^* T/B}{\sinh(\alpha m^* T/B)}, \quad (1)$$

where A_0 is a prefactor, $\alpha = 2\pi^2 k_B m_e / e\hbar = 14.69 \text{ T/K}$, k_B and \hbar the Boltzmann and Planck constants, e the electron charge, and B is taken as the harmonic mean of the oscillatory field range. This LK fit gives the effective mass m^* in units of the free-electron mass m_e of the carrier for that orbit.

The observation of QO requires high-purity crystals

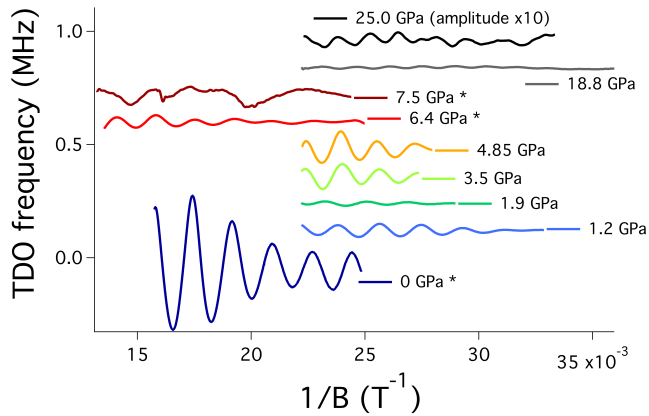


Figure 7: TDO frequency vs inverse field at base ^3He temperatures for various pressures, vertically shifted for clarity. The data indicated with an asterisk were taken in pulsed magnetic fields.

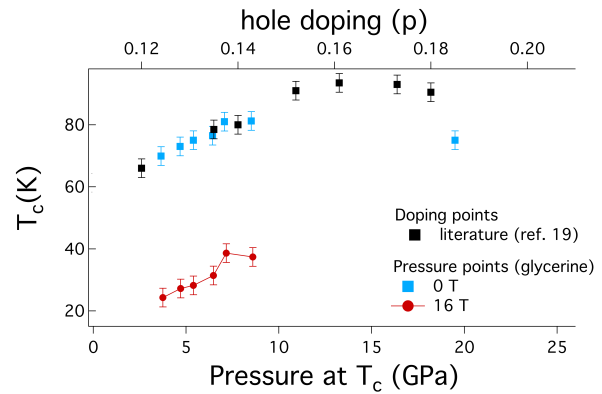
with minimal scattering, and hydrostatic conditions. Despite non-hydrostatic conditions for the cells at pressure higher than 15 GPa, clear QO are observed in Fig. 4, with their temperature evolution in Fig. 5. The high bulk modulus of YBCO makes it less susceptible to strains due to pressure gradients as suggested by Tateiwa *et al.* [28]. Figure 7 shows the oscillatory part of the TDO signal at about 400 mK for various pressures as a function of $1/B$, with the 25 GPa curve multiplied by 10 for better visibility. Comparable SdH frequencies are observed throughout the pressure range.

DISCUSSION

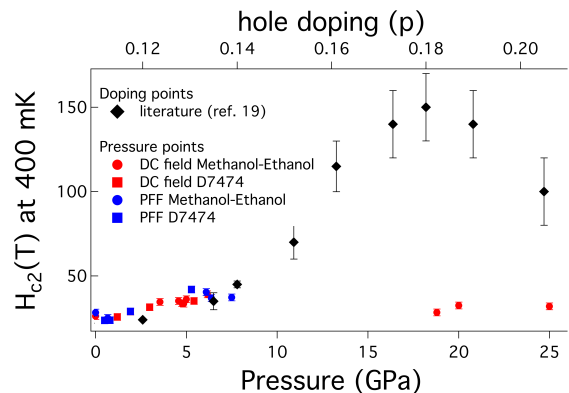
Figure 8(a) shows the evolution of T_c with pressure, increasing from 69.9 K at 3.65 GPa up to 81.2 K at 8.5 GPa. This yields a $dT_c/dP \approx 2.3$ K/GPa, in agreement with previous studies ([29], [30], [31]). Previous attempts to explain the evolution of the superconducting transition with pressure P ([32], [31]) invoke two main mechanisms described by:

$$\frac{dT_c}{dP} = \left(\frac{\partial T_c}{\partial n_h}\right)\left(\frac{\partial n_h}{\partial P}\right) + \left(\frac{dT_c}{dP}\right)_{intrinsic}, \quad (2)$$

The first term on the right-hand side accounts for an increase of T_c due to an increase in hole doping n_h via a charge transfer between the CuO chains and the CuO plane. The second term encompasses intrinsic effects, such as the increase of oxygen ordering in the CuO chains upon pressure. These intrinsic effects have been extensively studied [29], and showed that the application of pressure at room temperature increases this ordering process, as opposed to applying the pressure at lower temperatures at which the oxygen chains are frozen. Following



(a)



(b)

Figure 8: (a) T_c as a function of pressure, at 0 and 16 T. The pressure is measured at $T=T_c$. (b) H_{c2} at base ^3He temperature as a function of pressure. The data points are separated depending on the pressure medium and magnet used. T_c and H_{c2} vs doping data taken from [19].

the reasoning of Cyr-Choinière *et al.* [30], we compare our dT_c/dP value to those reported by studies in which those effects are minimized, and find a comparable value of dT_c/dP . In order to estimate the change of doping with pressure, thus, we neglect the intrinsic pressure effects on T_c .

Previous studies have attempted to quantify the change in doping with applied pressure:

$$n_h(P) = n_{h,0} + \frac{dn_h(P)}{d\epsilon(P)}\epsilon(P), \quad (3)$$

where $n_{h,0}$ is the initial hole doping (also denoted p), and $\epsilon(P)$ is the change in unit-cell volume. We apply the first-order Murnaghan equation of state [33], [21]:

$$\frac{dn_h(P)}{d\epsilon(P)} = n'_h(P)B_0\left(1 + \frac{B'_0}{B_0}P\right)^{1+1/B'_0}, \quad (4)$$

$$\epsilon(p) = 1 - \left(1 + \frac{B'_0}{B_0}p\right)^{-1/B'_0}, \quad (5)$$

where B_0 is the bulk modulus and B'_0 its pressure derivative at zero pressure, and $n'_h = dn_h(P)/d(P)$. Comparing our point of $T_c=81$ K at 7.07 GPa, with reported T_c values as a function of doping [19], we estimate the hole doping at that pressure to be of the order of $n_h(7.07 \text{ GPa}) = 0.142$ holes/Cu. Using approximation of values reported from x-ray diffraction data and calculations for various neighboring dopings of YBCO [34], we use $B_0 \approx 140 \pm 15$ GPa, and $B'_0 \approx 5.5 \pm 0.1$, which yields $dn_h(P)/d(P)(7.07 \text{ GPa}) \approx 0.37 \pm 0.1\%$ hole/GPa, in agreement with recent NMR studies [31].

Figure 8(b) shows the evolution of H_{c2} with pressure, along with a comparison of the evolution in doping (data points from [19] and references therein). The pressure-doping comparison is consistent at pressures below 8 GPa. Our initial decrease in H_{c2} with a minimum at 0.8 GPa is consistent with the minimum in H_{c2} observed near $p=0.12$. The $H_{c2}=28.4$ T observed for 18.8 GPa places this sample on the overdoped side of the YBCO superconducting dome, making it the first direct measurement of the critical field of overdoped YBCO. The pressure-doping equivalence previously estimated gives $p \approx 0.18$. Our H_{c2} value is, however, in discrepancy with previous measurements reporting $H_{c2}=150 \pm 20$ T for this doping. Comparing reported H_{c2} values with ours would indicate a doping near $p=0.24$. The pressure-doping equivalence calculated clearly breaks down at higher pressure, possibly indicating that intrinsic effects, which we neglected, should be taken into account. Those effects can create strains along the different axes of the sample. Several studies have looked into uniaxial compression effects on YBCO. Kim *et al.*, in particular [11], have suggested a three-dimensional charge order upon compression of the a -axis in zero magnetic field. Thus, one option to explain the discrepancy observed in H_{c2} which could be investigated by high pressure NMR, would be the existence of a competing charge order created at non-hydrostatic high pressures akin to strain.

Figure 9(a) and (b) show, respectively, the evolution of the QO frequency and their effective masses with pressure. The data points for comparison with doping are taken from [18] and references within. The QO frequency range observed in our study, 550-650 T, is in excellent agreement with reported data. We observe a minimum in frequency at 0.8 GPa, similar to that observed in H_{c2} , and a possible maximum near 6 GPa. The values are consistent between DC field and pulsed-field measurements, and no clear influence of the pressure medium is observed. The m^* obtained from LK fits are in the range of 1.5-2.5 m_e , also in agreement with reported data. We note a minimum in m^* near 4 GPa. Our low-pressure range does not extend far enough in p to observe the divergence in m^* noted by Ramshaw *et al.* [18]. The frequencies obtained for pressures greater than 18 GPa in the overdoped regime are, however, in complete discrepancy with the literature for the Tl analog. We obtain 710 ± 10 T for 18.8

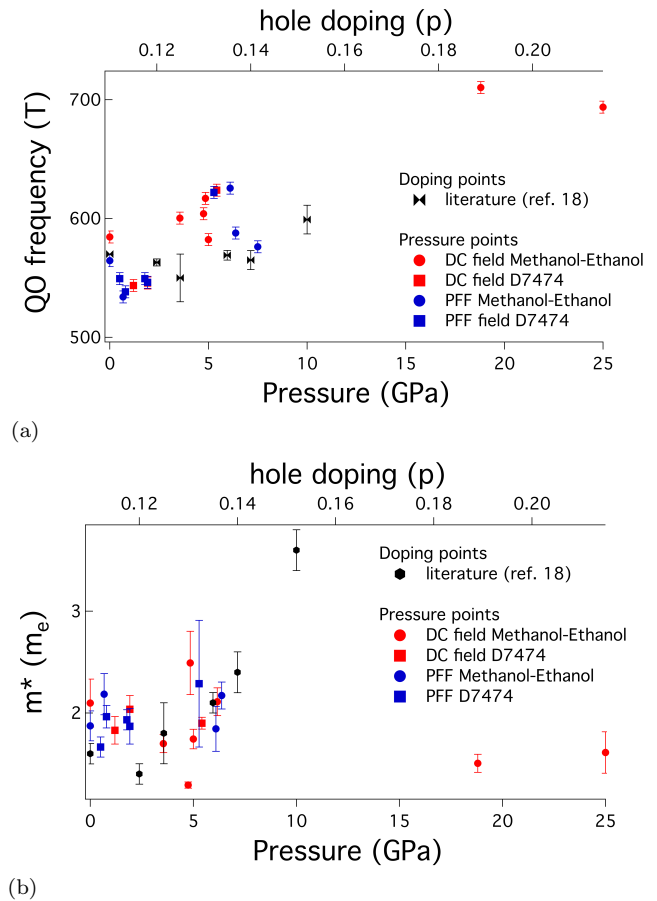


Figure 9: (a) QO frequencies measured vs pressure. (b) Effective masses m^* vs pressure. The doping data points are taken from [18].

GPa, and 694 ± 10 T at 25 GPa. The corresponding m^* are $1.50 \pm 0.08 m_e$ and $1.6 \pm 0.2 m_e$, respectively. This is in disagreement with the proposed picture of a Fermi-surface reconstruction for overdoped samples based on measurements of $\text{Tl}_2\text{Ba}_2\text{CuO}_{6+\delta}$, that were shown by angle-dependent magnetoresistance oscillations (AMRO) [13], [35] and ARPES measurements [36], [37] to have a large coherent three-dimensional Fermi surface. Resistivity and torque measurements at ambient pressure [38] have revealed QOs with a frequency of $18 \text{ kT} \pm 50 \text{ T}$ and an effective mass $m^* = 4.1 \pm 1.0 m_e$. The low H_{c2} values at high pressure, and negligible change in QOs frequency from low to high pressures do not support the picture of a FSR across the superconducting dome, and rather point to the existence of a charge order similar to the one observed at low pressure and on the underdoped side.

CONCLUSION

Our high pressure TDO measurements of YBCO_{6.5} have enabled direct measurement of T_c , H_{c2} , and QOs,

from which we derived QO frequencies and effective masses. Measurements at pressures below 8 GPa show results in excellent agreement with previous doping studies, confirming the equivalence of pressure and doping. We estimated the value for a charge transfer with pressure and found it to be compatible with other data [31]. The pressure dependences of H_{c2} and the QO frequency indicates also a suppression of the CO by applied pressure. By applying pressures larger than 18 GPa, the sample was driven to the overdoped regime on the other side of the superconducting dome, as shown by the measured values of T_c and H_{c2} . However, the QO frequency measured, comparable to those obtained in the lower pressure range, do not support the picture of a FSR in the overdoped regime of YBCO, but rather indicate the existence of a charge order in competition with the superconducting state. High pressure x-ray and NMR should shed light on the origin of this CO and inform on its links to the low pressure, low-doping ones reported.

This work was funded by the DOE/NNSA under DE-NA0001979 and was performed at the National High Magnetic Field Laboratory, which is supported by NSF Cooperative Agreement No. DMR-1157490 and by the State of Florida. Part of this work was supported as part of the Center for Actinide Science and Technology (CAST), an Energy Frontier Research Center funded by the U.S. Department of Energy, Office of Science, Basic Energy Sciences under Award No. DE-SC0016568, and by the Deutsche Forschungsgemeinschaft (DFG) through the Würzburg-Dresden Cluster of Excellence on Complexity and Topology in Quantum Matter—ct.qmat (EXC 2147, Grant No. 390858490). We acknowledge the support of HLD at HZDR, a member of the European Magnetic Field Laboratory (EMFL). ADG, WAC and SWT thank J. Wosnitza for financial support and careful review of the manuscript. ADG acknowledges N. Doiron-Leyraud and S. Badoux for stimulating discussions, and C. Agosta for crucial help in the data analysis. SWT thanks D. Schiferl for bringing the Parmax and Zylon to his attention.

-
- * stan.tozer@magnet.fsu.edu
† a.grockowiak@ifw-dresden.de
- [1] M. K. Wu, J. R. Ashburn, C. J. Torng, P. H. Hor, R. L. Meng, L. Gao, Z. J. Huang, Y. Q. Wang, and C. W. Chu, *Phys. Rev. Lett.* **58**, 908 (1987).
 - [2] L. Taillefer, *J. Condens. Matter Phys.* **21**, 164212 (2009).
 - [3] D. LeBoeuf, N. Doiron-Leyraud, J. Levallois, R. Daou, J.-B. Bonnemaïson, N. E. Hussey, L. Balicas, B. J. Ramshaw, R. Liang, D. A. Bonn, W. N. Hardy, S. Adachi, C. Proust, and L. Taillefer, *Nature* **450**, 533 (2007).
 - [4] D. LeBoeuf, N. Doiron-Leyraud, B. Vignolle, M. Sutherland, B. J. Ramshaw, J. Levallois, R. Daou, F. Laliberté, O. Cyr-Choinière, J. Chang, Y. J. Jo, L. Balicas, R. Liang, D. A. Bonn, W. N. Hardy, C. Proust, and L. Taillefer, *Phys. Rev. B* **83**, 054506 (2011).
 - [5] J. Chang, R. Daou, C. Proust, D. LeBoeuf, N. Doiron-Leyraud, F. Laliberté, B. Pingault, B. J. Ramshaw, R. Liang, D. A. Bonn, W. N. Hardy, H. Takagi, A. B. Antunes, I. Sheikin, K. Behnia, and L. Taillefer, *Phys. Rev. Lett.* **104**, 057005 (2010).
 - [6] T. Wu, H. Mayaffre, S. Kramer, M. Horvatić, C. Berthier, W. N. Hardy, R. Liang, D. A. Bonn, and M.-H. Julien, *Nature* **477**, 191 (2011).
 - [7] J. Chang, E. Blackburn, A. T. Holmes, N. B. Christensen, J. Larsen, J. Mesot, R. Liang, D. A. Bonn, W. N. Hardy, A. Watenphul, M. v. Zimmermann, E. M. Forgan, and S. M. Hayden, *Nat. Phys.* **8**, 871 (2012).
 - [8] S. Gerber, H. Jang, H. Nojiri, S. Matsuzawa, H. Yasumura, D. A. Bonn, R. Liang, W. N. Hardy, Z. Islam, A. Mehta, S. Song, M. Sikorski, D. Stefanescu, Y. Feng, S. A. Kivelson, T. P. Devereaux, Z.-X. Shen, C.-C. Kao, W.-S. Lee, D. Zhu, and J.-S. Lee, *Science* **350**, 949 (2015).
 - [9] F. Laliberté, M. Frachet, S. Benhabib, B. Borgnic, T. Loew, J. Porras, M. Le Tacon, B. Keimer, S. Wiedmann, C. Proust, and D. LeBoeuf, *npj Quantum Mater.* **3**, 11 (2018).
 - [10] T. Wu, H. Mayaffre, S. Krämer, M. Horvatić, C. Berthier, P. L. Kuhns, A. P. Reyes, R. Liang, W. N. Hardy, D. A. Bonn, and M.-H. Julien, *Nat. Comm.* **4**, 2113 (2013).
 - [11] H.-H. Kim, S. M. Souliou, M. E. Barber, E. Lefrançois, M. Minola, M. Tortora, R. Heid, N. Nandi, R. A. Borzi, G. Garbarino, A. Bosak, J. Porras, T. Loew, M. König, P. J. W. Moll, A. P. Mackenzie, B. Keimer, C. W. Hicks, and M. Le Tacon, *Science* **362**, 1040 (2018).
 - [12] N. Doiron-Leyraud, C. Proust, D. LeBoeuf, J. Levallois, J.-B. Bonnemaïson, R. Liang, D. A. Bonn, W. N. Hardy, and L. Taillefer, *Nature* **447**, 565 (2007).
 - [13] N. E. Hussey, M. Abdel-Jawad, A. Carrington, A. P. Mackenzie, and L. Balicas, *Nature* **425**, 814 (2003).
 - [14] B. Vignolle, A. Carrington, R. A. Cooper, M. M. J. French, A. P. Mackenzie, C. Jaudet, D. Vignolles, C. Proust, and N. E. Hussey, *Nature* **455**, 952 (2008).
 - [15] N. Barišić, M. K. Chan, Y. Li, G. Yu, X. Zhao, M. Dreschel, A. Smontara, and M. Greven, *Proc. Natl. Acad. Sci. U.S.A.* **110**, 12235 (2013).
 - [16] M. A. Hossain, J. D. F. Mottershead, D. Fournier, A. Bostwick, J. L. McChesney, E. Rotenberg, R. Liang, W. N. Hardy, G. A. Sawatzky, I. S. Elfimov, D. A. Bonn, and A. Damascelli, *Nat. Phys.* **4**, 527 (2008).
 - [17] T. Helm, M. V. Kartsovnik, M. Bartkowiak, N. Bittner, M. Lambacher, A. Erb, J. Wosnitza, and R. Gross, *Phys.*

- Rev. Lett. **103**, 157002 (2009).
- [18] B. J. Ramshaw, S. E. Sebastian, R. D. McDonald, J. Day, B. S. Tan, Z. Zhu, J. B. Betts, R. Liang, D. A. Bonn, W. N. Hardy, and N. Harrison, *Science* **348**, 317 (2015).
- [19] G. Grissonnanche, O. Cyr-Choinière, F. Laliberté, S. René de Cotret, A. Juneau-Fecteau, S. Dufour-Beauséjour, M. È. Delage, D. LeBoeuf, J. Chang, B. J. Ramshaw, D. A. Bonn, W. N. Hardy, R. Liang, S. Adachi, N. E. Hussey, B. Vignolle, C. Proust, M. Sutherland, S. Krämer, J. H. Park, D. Graf, N. Doiron-Leyraud, and L. Taillefer, *Nat. Comm.* **5**, 3280 (2014).
- [20] J. L. Tallon, C. Bernhard, G. V. M. Williams, and J. W. Loram, *Phys. Rev. Lett.* **79**, 5294 (1997).
- [21] P. L. Alireza, G. H. Zhang, W. Guo, J. Porras, T. Loew, Y.-T. Hsu, G. G. Lonzarich, M. Le Tacon, B. Keimer, and S. E. Sebastian, *Phys. Rev. B* **95**, 100505 (2017).
- [22] S. Sadewasser, Y. Wang, J. S. Schilling, H. Zheng, A. P. Paulikas, and B. W. Veal, *Phys. Rev. B* **56**, 14168 (1997).
- [23] S. W. Tozer, A. W. Kleinsasser, T. Penney, D. Kaiser, and F. Holtzberg, *Phys. Rev. Lett.* **59**, 1768 (1987).
- [24] S. W. Tozer, J. L. Koston, and E. M. McCarron III, *Phys. Rev. B* **47**, 8089 (1993).
- [25] D. E. Graf, R. L. Stillwell, K. M. Purcell, and S. W. Tozer, *High Pressure Research* **31**, 533 (2011).
- [26] A. Savitzky and M. J. E. Golay, *Analytical Chemistry* **36**, 1627 (1964).
- [27] D. Schoenberg, *Magnetic Oscillations in Metals* (Cambridge University Press, 2009).
- [28] N. Tateiwa and Y. Haga, *Rev. Sci. Instr.* **80**, 123901 (2009).
- [29] S. Sadewasser, J. S. Schilling, A. P. Paulikas, and B. W. Veal, *Phys. Rev. B* **61**, 741 (2000).
- [30] O. Cyr-Choinière, D. LeBoeuf, S. Badoux, S. Dufour-Beauséjour, D. A. Bonn, W. N. Hardy, R. Liang, D. Graf, N. Doiron-Leyraud, and L. Taillefer, *Phys. Rev. B* **98**, 064513 (2018).
- [31] M. Jurkutat, C. Kattinger, S. Tsankov, R. Reznicek, A. Erb, and J. Haase, *Proc. Natl. Acad. Sci. U.S.A.* **120**, e2215458120 (2023).
- [32] S. Kawasaki, Z. Li, M. Kitahashi, C. T. Lin, P. L. Kuhns, A. P. Reyes, and G.-q. Zheng, *Nat. Comm.* **8**, 1267 (2017).
- [33] J. S. Olsen, S. Steenstrup, L. Gerward, and B. Sundqvist, *Phys. Scr.* **44**, 211 (1991).
- [34] H. A. Ludwig, W. H. Fietz, and H. Wühl, *Physica C Supercond* **197**, 113 (1992).
- [35] M. Abdel-Jawad, M. P. Kennett, L. Balicas, A. Carrington, A. P. Mackenzie, R. H. McKenzie, and N. E. Hussey, *Nat. Phys.* **2**, 821 (2006).
- [36] A. Damascelli, D. H. Lu, and Z.-X. Shen, *Journal of Electron Spectroscopy and Related Phenomena* **117**, 165 (2001).
- [37] M. Platié, J. D. F. Mottershead, I. S. Elfimov, D. C. Peets, R. Liang, D. A. Bonn, W. N. Hardy, S. Chiuzbajian, M. Falub, M. Shi, L. Patthey, and A. Damascelli, *Phys. Rev. Lett.* **95**, 077001 (2005).
- [38] B. Vignolle, D. Vignolles, D. LeBoeuf, S. Lepault, B. Ramshaw, R. Liang, D. A. Bonn, W. N. Hardy, N. Doiron-Leyraud, A. Carrington, N. E. Hussey, L. Taillefer, and C. Proust, *Comptes Rendus Physique* **12**, 446 (2011).
- [39] C. T. Van Degrift, *Rev. Sci. Instr.* **46**, 599 (2019).
- [40] W. A. Coniglio, L. E. Winter, C. Rea, K. Cho, and C. Agosta, *arXiv* (2010), 1003.5233v1.
- [41] S. Zherlitsyn, B. Wustmann, T. Herrmannsdorfer, and J. Wosnitzer, *IEEE Transactions on Applied Superconductivity* **22**, 4300603 (2012).
- [42] R. A. Forman, G. J. Piermarini, J. D. Barnett, and S. Block, *Science* **176**, 284 (1972).
- [43] S. Klotz, J.-C. Chervin, P. Munsch, and G. L. Marchand, *Journal of Physics D: Applied Physics* **42**, 075413 (2009).

SUPPLEMENTARY INFORMATION

Tuned LC tank circuit The tunnel-diode-oscillator (TDO) technique is a RLC tank circuit driven by a tunnel diode oscillator as described in Ref. [39] and [40]. The inductor coil inside the sample space of the pressure cell is shown in Sup. Fig. 4. The diode card, consisting of the tunnel diode, capacitors and resistor, is located at cryogenic temperatures 3 cm above the sample. This reduces the capacitance of the circuit between the diode and the sample, ensuring a larger signal, and allows us to drive the circuit at a higher frequency so that the change in frequency is larger. The resonant frequency measures the skin depth for a metal and the penetration depth of a superconductor. The portion of the sample actually measured is proportional to the inverse resonant frequency and the resistivity of the sample, according to:

$$\delta = \sqrt{\frac{\rho}{\pi f \mu}}, \quad (6)$$

where δ is the RF skin depth probed, ρ the resistivity, f the frequency, and μ the permeability. Taking $\mu = \mu_0$ for a conductor, f of the order of 500 MHz and ρ on the order of 0.1 m Ω .cm above T_c for a hole concentration p of 0.09 [15], we obtain a skin depth on the order of 20 μ m. The typical sample dimensions are 100x100x20 μ m³. Therefore, we are able to probe the entire thickness of the YBCO sample, while maintaining efficient coupling between the skin depth and inductor. It must be noted that the power dissipated by the TDO circuit at the sample at base ³He temperatures, combined with the low thermal conductivity in a pressure cell due to a glassy pressure medium, led to discrepancies between the temperature measured and the actual sample temperature. The power dissipated by the TDO card has been estimated to be less than 10 μ W which would not affect the LK fits, that rely more heavily on the higher temperature points.

High pressure This high pressure study of YBCO6.5 was performed using custom-made diamond anvil cells (DACs) based on the turnbuckle design as described in Ref. [25]. Various cells that make use of that concept are shown in Sup. Fig. 1. Non-magnetic metallic DACs (BeCu C17200) were used for the static DC magnetic field measurements. Measurements in pulsed magnetic

fields at ^3He temperatures require additional precautions to limit the vibrations and heating generated by the high dB/dt . The rapidly increasing field on the upsweep of a 70 T coil is of the order of 2400 T/s, and, respectively, 770 and 19000 T/s for outsert and insert of the 85 T duplex coil at HLD-EMFL [41]. To limit these deleterious effects, our DACs and rotators for pulsed-field studies are made of the plastic Parmax (SRP120) [25], a high strength self-reinforced polymer; the ^3He and ^4He cryostat tails are made from spiral-wound 75 μm thick G10 sheets. Any heating would result in an offset between the up- and downsweep traces and a diminished amplitude of the QO. As shown in Fig. 3 by the near perfect overlap of the upsweep and downsweep traces, negligible heating of the sample occurs during a pulse at ^3He base temperature.

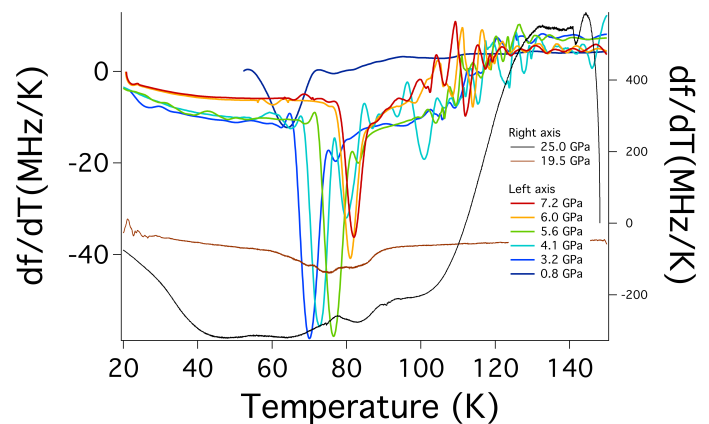
As shown in Sup. Fig. 1, our DACs have been designed to be rotated in the constrained space of magnet bores at cryogenic temperatures (32 mm for DC field; 15.5 mm for pulsed magnets), which enables us to carefully align our samples in field and carry out angular dependence studies.

Supplementary Figure 4 shows a typical TDO DAC set up. The gaskets used are composed of two parts: an insulating blend of diamond powder and epoxy compressed between the anvils, and a ring epoxied around the culet to hold that mix. That ring is made of either radially-wound Zylon fiber for the plastic cells or a stainless-steel 304 gasket for the metallic cells. The stainless-steel gaskets were pre-indented, and the indented region drilled out and filled with the diamond powder and epoxy mix. Various culet sizes were used, from 450 to 800 μm , depending on the desired maximum pressure. For pressures below 10 GPa, the typical geometry of our hand-wound TDO coils is a three-turn coil, with an ID of 100-150 μm made using AWG56 (12 μm) or AWG59 (9 μm) copper wire with polynylon insulation. For pressures greater than 10 GPa, 2-turn coils were used to have more height available in the sample space to compress the gasket. Reducing the number of turns in the coil reduces the amplitude of the TDO signal (see results in Fig. 7).

Ruby spheres (RSA Le Rubis) are placed in the sample space of the DAC. A 532 nm laser was used to excite the R1 and R2 lines of the ruby. This enabled systematic measurements of the pressure at low temperature with an optical fiber placed against the upper diamond anvil. For T_c measurements, the pressure is also measured at the onset temperature of superconductivity since the pressure changes with temperature. An additional optical fiber with ambient ruby is located in close proximity to the DAC to account for the temperature dependence of the ruby fluorescence. Laser power is minimized to avoid any heating of the ruby during the pressure measurement. The value of the pressure is given by $p = (\text{cell R1} - \text{ambient R1}) (\text{nm}) / 0.365 (\text{nm/GPa})$ [42]. Several pressure media were utilized; glycerin, Daphne

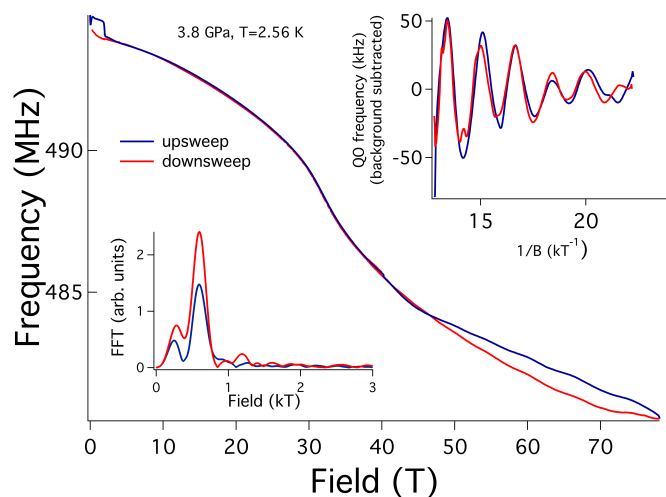


Supplementary Figure 1: Various turnbuckle DACs, from left to right: 6 mm diameter DAC for MPMS work, large-angle DAC for optical and x-ray studies, EC17 model made of black Parmax (the metallic version of which was used for our DC field studies), EC15b model made of Parmax, and the EC15b cell in a plastic pulsed-field rotator.

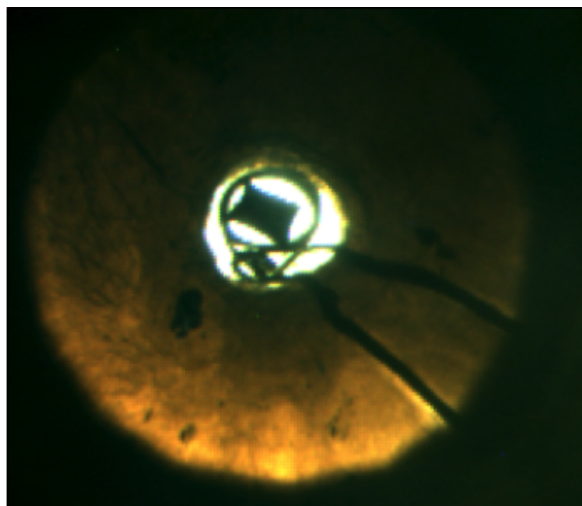


Supplementary Figure 2: Derivative of the TDO frequency of the data in Fig.1. The minima around 80 K are the T_c , and clearly appears at about 74.5 K at 19.5 GPa

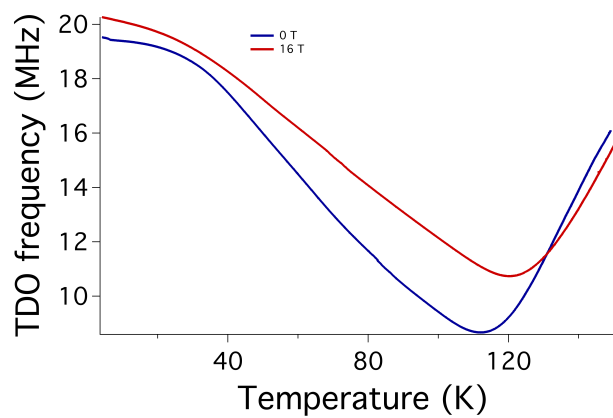
7474, and a mixture of 4:1::methanol:ethanol for pressures greater than 5 GPa. Different pressure media have different hydrostatic limits (see [28], [43]), and these decrease with decreasing temperatures. The hydrostatic limit for 4:1::methanol:ethanol is 10 GPa at room temperature, which means that our pressures greater than 18 GPa are quasi-hydrostatic. The hydrostaticity level within a cell under pressure is monitored by observing the FWHM of the ruby fluorescence lines. Non-hydrostatic conditions strain the sample and create a condition similar to scattering which can suppress QOs.



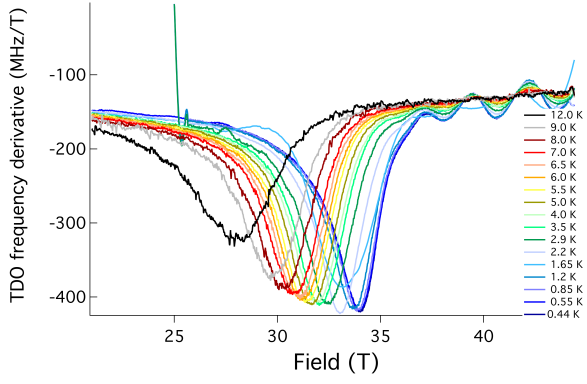
Supplementary Figure 3: Main panel: TDO frequency vs field for a sample at 2.56 K and 3.8 GPa, taken in the 85 T duplex coil at HLD-EMFL. Top right panel: oscillatory part, background-subtracted vs $1/B$. Bottom left panel: Fourier transformation of the signal shown in the top right panel.



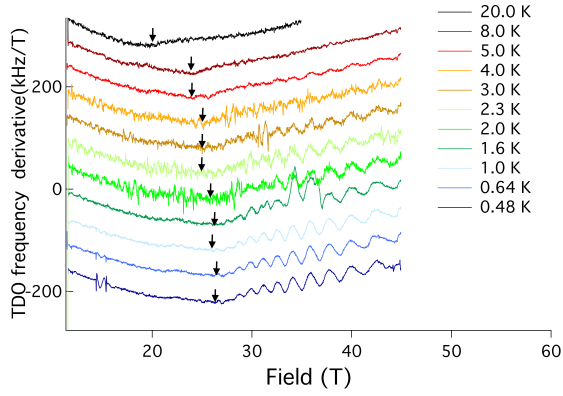
Supplementary Figure 4: Image taken through the diamond anvil of the 25 GPa cell, which shows a typical TDO DAC set up - the rectangular sample can be seen in the coil which resides in the clear space of the gasket filled with 4:1::methanol:ethanol pressure medium with the coil leads coming out over the insulating insert of the gasket. The circular, semi-transparent area around the sample space is the diamond powder and epoxy gasket, and the darker region is the metallic ring confining it. A few ruby spheres can be distinguished between the top part of the coil and the gasket.



Supplementary Figure 5: Evolution of the TDO frequency as a function of temperature for the 25 GPa cell, at 0 and 16 T. The broad feature observed in the 0 T trace cannot be interpreted as the superconducting transition widened by non-hydrostatic conditions as an applied field of 16 T does not shift it to lower temperatures.

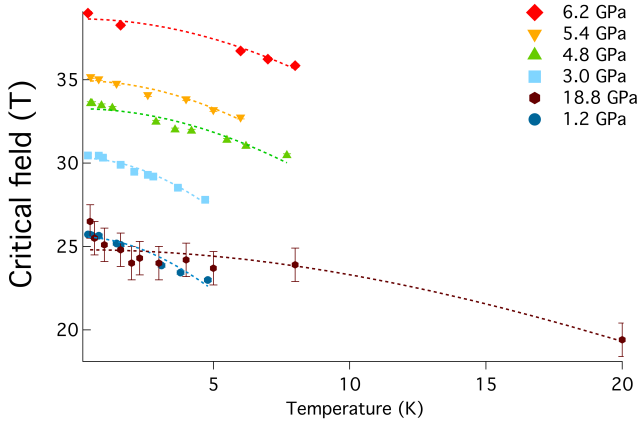


(a)



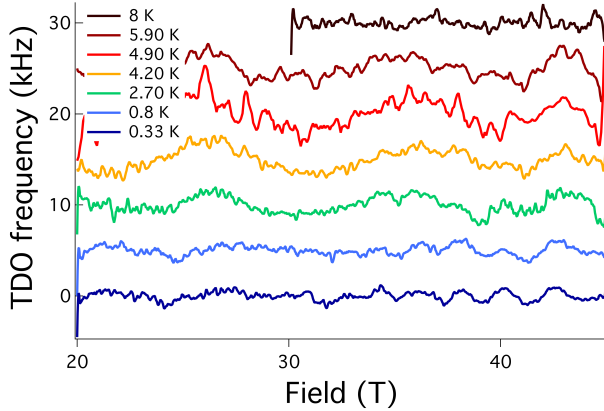
(b)

Supplementary Figure 6: (a) derivative of the TDO frequency vs field at 4.7 GPa for various temperatures. The critical field is clearly identified as the minimum in the derivative, followed by the onset of quantum oscillations. (b) derivative of the TDO frequency vs field at 18.8 GPa. The minimum in the derivative, compared with that obtained for 4.7 GPa, followed by the onset of quantum oscillations, is interpreted as the critical field at this pressure and is indicated by arrows.



Supplementary Figure 7: Evolution of the upper critical field as a function of temperature for several pressures.

The dotted lines are GL fits. The minimum in the derivative defined as H_{c2} observed at 28.4 T (Fig. 4) for 18.8 GPa is plotted here along with data from the same feature found at lower pressures and seems to follow the similar trend.



Supplementary Figure 8: Background-subtracted TDO frequencies at 25 GPa, showing the temperature evolution of the QO amplitudes, existing up to 2.7 K. The traces are vertically shifted for clarity.